International Journal of Biological Macromolecules 350 (2026) 151039

Contents lists available at ScienceDirect

International Journal of Biological Macromolecules

journal homepage: www.elsevier.com/locate/ijbiomac

Chitosan–calcium–simvastatin scaffold for bone repair under inflammation

Marjorie de Oliveira Gallinari [a,d], Ester Alves Ferreira Bordini [b], Elisa Mara de Abreu Furquim [c], Priscila Toninatto Alves de Toledo [a], Vitor de Toledo Stuani [a], Ruan Henrique Delmonica Barra [c], Edilson Ervolino [d], Luciano Tavares Angelo Cintra [e], Carlos Alberto de Souza Costa [f], Juliano Milanezi de Almeida [c], Diana Gabriela Soares [a,*]

[a] Department of Operative Dentistry, Endodontics and Dental Materials, Bauru School of Dentistry, University of São Paulo (USP), Alameda Dr. Octávio Pinheiro Brisolla, 9-75, Bauru, São Paulo, 17012-901, Brazil
[b] Department of Dental Materials and Prosthodontics, Ribeirão Preto School of Dentistry, University of São Paulo (USP), Av. do Café - Subsetor Oeste - 11 (N-11), Ribeirão Preto, São Paulo, 14040-904, Brazil
[c] Department of Diagnosis and Surgery, School of Dentistry of Araçatuba, São Paulo State University (UNESP), Street José Bonifácio, 1193 - Vila Mendonca, Araçatuba, São Paulo, 16015-050, Brazil
[d] Department of Basic Sciences, School of Dentistry of Araçatuba, São Paulo State University (UNESP), Street José Bonifácio, 1193 - Vila Mendonca, Araçatuba, São Paulo, 16015-050, Brazil
[e] Department of Operative Dentistry, School of Dentistry of Araçatuba, São Paulo State University (UNESP), Street José Bonifácio, 1193 - Vila Mendonca, Araçatuba, São Paulo, 16015-050, Brazil
[f] Department of Physiology and Pathology, School of Dentistry of Araraquara, São Paulo State University (UNESP), Street Humaitá, 1680, Araraquara, São Paulo, 14801-385, Brazil

ARTICLE INFO

Key-words:
Chitosan scaffold
Calcium hydroxide
Simvastatin
Inflammation modulation
Bone regeneration

ABSTRACT

Regenerating mineralized tissues under degenerative inflammatory stimuli is challenging, as elevated pro-inflammatory mediators impair the reparative capacity of resident cells. This study developed a chitosan-based scaffold functionalized with calcium hydroxide and simvastatin to modulate inflammation and enhance bone regeneration in inflammatory conditions. Scaffolds were fabricated from 2% chitosan, with or without Ca $(OH)_2$, and incubated in 1 μM simvastatin, generating four formulations: CH, CH-Ca, CH-SV, and CH-Ca-SV. In vitro, SAOS-2 cells were preconditioned in serum-free medium with or without TNF-α (100 ng/mL) for three days to simulate a degenerative inflammatory microenvironment. Cell metabolic activity, expression of inflammatory genes, alkaline phosphatase activity, mineralized matrix deposition, and osteogenic gene expression were assessed. In vivo, critical-size calvarial defects were created in Wistar rats, with or without TNF-α-induced osteolytic lesions, and filled with blood clot (control), CH-Ca, or CH-Ca-SV. After 14 and 30 days, samples were analyzed by micro-computed tomography, histology, and immunohistochemistry (IL-1β, TNF-α). In vitro, CH-SV and CH-Ca-SV extracts significantly increased cell metabolic activity, enhanced osteogenic differentiation, and downregulated TNF-α, MMP9, and IL-1β under inflammatory challenge. In vivo, CH-Ca-SV scaffolds promoted greater bone formation, reduced inflammatory infiltrate, and improved scaffold integrity compared to CH-Ca. Immunohistochemistry confirmed higher cytokine expression in control defects. Overall, simvastatin-loaded chitosan–calcium scaffolds effectively modulate inflammation and enhance bone regeneration even in a pro-inflammatory environment, supporting their potential for treating inflammatory bone defects.

1. Introduction

The advances in regenerative approaches to regenerate mineralized tissues have been largely driven by the development of biomaterials capable of biostimulation of the patient's resident cells. However, it is important to highlight that most of these studies are conducted under conditions of cell and tissue homeostasis, which is not representative of the clinical conditions where regeneration is required. Often, tissue loss is triggered by a persistent local inflammatory reaction, and its severity can negatively affect the repair process [1]. Thus, it can be easily

* Corresponding author at: Department of Operative Dentistry, Endodontics and Dental Materials, Bauru School of Dentistry, University of São Paulo - USP, Alameda Doutor Octávio Pinheiro Brisolla, 9-75, Bauru, SP, Brazil.
E-mail address: dianasoares@fob.usp.br (D.G. Soares).

https://doi.org/10.1016/j.ijbiomac.2026.151039
Received 1 December 2025; Received in revised form 9 February 2026; Accepted 19 February 2026
Available online 20 February 2026

implied that tissue engineering therapies developed for these applications should include strategies that mitigate the deleterious potential of the inflammatory reaction and facilitate the performance of resident precursor cells [1,2].

One of these strategies is the improvement of biomaterials through the incorporation of agents with known biological activity. Therefore, tissue regeneration can be enhanced through modifications in the mechanisms of chemotaxis, angiogenesis, cell differentiation and inflammatory reaction. In this context, statins, a class of drugs used to control cholesterol synthesis through competitive inhibition of the mevalonate pathway, have aroused great interest as adjuvants in bone and dentin regeneration [3–5]. This interest is due to the pleiotropic effect of the drug, where its ability to induce osteoblastic and odontoblastic phenotype in progenitor cells from bone marrow and pulp tissue is observed [6–11].

Several studies have shown that statins can also modulate inflammation in different tissues and stimulate mineralized tissue deposition in vitro and in vivo [11–19]. These effects are dose-dependent, with concentrations between 0.01 and 1 μM/L being able to induce osteo-/odontogenic differentiation of progenitor cells and favor mineralization through stimulation of the ERK1/2 and Smad1/2/3 signaling pathways, associated with increased BMP-2 expression, in a mechanism independent of the mevalonate pathway. In contrast, the anti-inflammatory effect of statins is more evident at higher doses (10 to 50 μM/L) and is mediated by several mechanisms, such as inhibition of the NF-kB pathway and increased expression of the transcription factor PPARγ.

In addition to bioactive drugs, calcium has a fundamental impact on bone regeneration and the formation of mineralized tissue. Calcium ions are essential regulators of osteoblast proliferation, differentiation, and extracellular matrix mineralization [20]. They act as both structural components of hydroxyapatite and signaling molecules that modulate cellular behavior. Studies have shown that calcium-enriched biomaterials enhance osteogenic differentiation, increase alkaline phosphatase activity, and promote the nucleation and growth of mineralized matrices [20,21]. Furthermore, calcium-containing scaffolds can modulate the local microenvironment by influencing ionic exchange and the cellular signaling pathways involved in bone remodeling [22]. This improves regenerative outcomes, especially under compromised or inflammatory conditions.

Due to the exposed properties, the scientific literature supports that the incorporation of statins in scaffolds enhances bone tissue regeneration in vitro and in vivo [17,22–32]. Similarly, they are able to modulate tertiary dentin deposition in cases of direct pulpal capping in vivo [33,34]. However, few studies have evaluated these pleiotropic effects of statins incorporated into scaffolds maintained in a microenvironment under degenerative inflammatory stimuli. As such, the objective of this study was to establish a therapeutic option for tissue engineering of mineralized tissues in degenerative inflammatory conditions using different chitosan scaffolds formulations that can release specific doses of statins, capable of minimizing the initial inflammatory reaction, and subsequently controlling the release of low concentrations of this drug. For this, an in vitro and in vivo degenerative inflammation model was established with the potential to negatively affect osteoblast activity through prior exposure to TNF-α, a pro-inflammatory mediator highly expressed in the main pathogen-mediated inflammatory lesions observed in the oral cavity.

2. Materials and methods

2.1. In vitro inflammatory model establishment

The osteoblastic SAOS-2 cell line was used in all experiments. Cells were cultured in Dulbecco's Modified Eagle's Medium (DMEM) supplemented with L-glutamine, 1% penicillin–streptomycin (GIBCO®, Invitrogen, USA), and 15% fetal bovine serum (FBS) under standard conditions (37 °C, 5% CO_2). The inflammatory microenvironment model was adapted from Soares et al. [35] to reproduce an in vitro degenerative stimulus capable of reducing calcium-rich matrix expression without negatively affecting cell viability. Briefly, 2000 SAOS-2 cells were seeded into 96-well plates (Corning®, New York, NY, USA) and incubated for 24 h. The culture medium was then replaced with DMEM supplemented with 100 ng/mL of TNF-α (TNF+), and the cells were maintained for 3 days. In the negative control (NC) group, cells were cultured in complete medium without TNF-α for the same period (TNF−). Subsequently, the culture medium was replaced with either regular or osteogenic medium (supplemented with 50 μg/mL ascorbic acid and 5 mM β-glycerophosphate, Sigma-Aldrich, St. Louis, MO, USA), and cells were cultured for up to 14 days (Fig. 1A). Cell viability (MTT assay) and mineralized matrix deposition (o-Cresolphthalein Complexone; OCC assay) were assessed immediately after TNF-α exposure (T0) and after 7 (T7) and 14 (T14) days of culture in osteogenic medium. For the MTT assay ($n = 6$), cells were incubated for 4 h with MTT solution (5 mg/mL; Sigma-Aldrich) diluted 1:10 in culture medium. Formazan crystals were dissolved in acidified isopropanol, and absorbance was measured at 570 nm (Synergy H1, Biotek, Winooski, VT, USA). For calcium quantification ($n = 6$), cells were incubated overnight at 4 °C with 50 μL of 1 N HCl, followed by the addition of 100 μL of OCC working reagent (Calcio Liquicolor, Centerkit, Campinas, SP, Brazil). Samples were incubated at room temperature for 10 min, and absorbance was recorded at 570 nm (Synergy H1, Biotek, Winooski, VT, USA). Calcium concentrations were determined using a standard curve. The NC group was considered as the 100% reference for each parameter and time point.

2.2. Selecting simvastatin dosage

After seeding SAOS-2 cells into 96-well plates, and following 24 h of incubation, cells were treated with simvastatin (SV; ≥97% HPLC, Sigma-Aldrich, St. Louis, MO, USA) at concentrations of 10, 5, 1, 0.1, and 0.01 μM for 1 or 3 days. Cell viability was evaluated using the MTT assay. To assess the anti-inflammatory potential of simvastatin, cells were cultured for 24 h and subsequently exposed to TNF-α (100 ng/mL) and/or SV (1 μM) for 3 days. Untreated cells served as negative controls (NC group). Expression levels of TNF-α, IL-1β, and MMP-9 were quantified by real-time PCR ($n = 6$). For evaluation of the osteogenic response under inflammatory conditions, SAOS-2 cells were pre-treated with TNF-α (100 ng/mL) for 3 days to induce an in vitro inflammatory state, and then cultured for 14 days in medium supplemented with 1 μM SV (Fig. 3A). The SV-supplemented medium was replaced every 48 h. At the end of the experimental period, cell viability (MTT assay; $n = 6$), alkaline phosphatase (ALP) activity (thymolphthalein monophosphate method; n = 6), and calcium deposition (OCC assay; n = 6) were determined. Gene expression of BMP-2, OCN, and OPN was analyzed by real-time PCR. (n = 6).

ALP activity was determined using the Alkaline Phosphatase Kit – End Point Assay (Labtest Diagnóstico S.A., Lagoa Santa, Minas Gerais, Brazil), as previously described by Soares et al. [36]. For real-time PCR, total RNA was extracted using the RNaqueous™ Micro Kit (Applied Biosystems, Foster City, CA, USA). An aliquot of 1 μg total RNA was used for cDNA synthesis with the High-Capacity cDNA Reverse Transcription Kit (Applied Biosystems). Relative quantification of gene expression was performed using the StepOnePlus™ Real-Time PCR System (Applied Biosystems) and TaqMan® assays, following the manufacturer's protocol. GAPDH served as the housekeeping gene. A total of 1 μL of cDNA was used per reaction in a 20 μL final PCR volume. The cycling conditions were as follows: 50 °C for 2 min, 95 °C for 10 min, followed by 40 cycles of 95 °C for 15 s and 60 °C for 1 min.

2.3. In vitro evaluation of simvastatin-loaded scaffolds under inflammatory conditions

The scaffolds were prepared according to the protocol previously

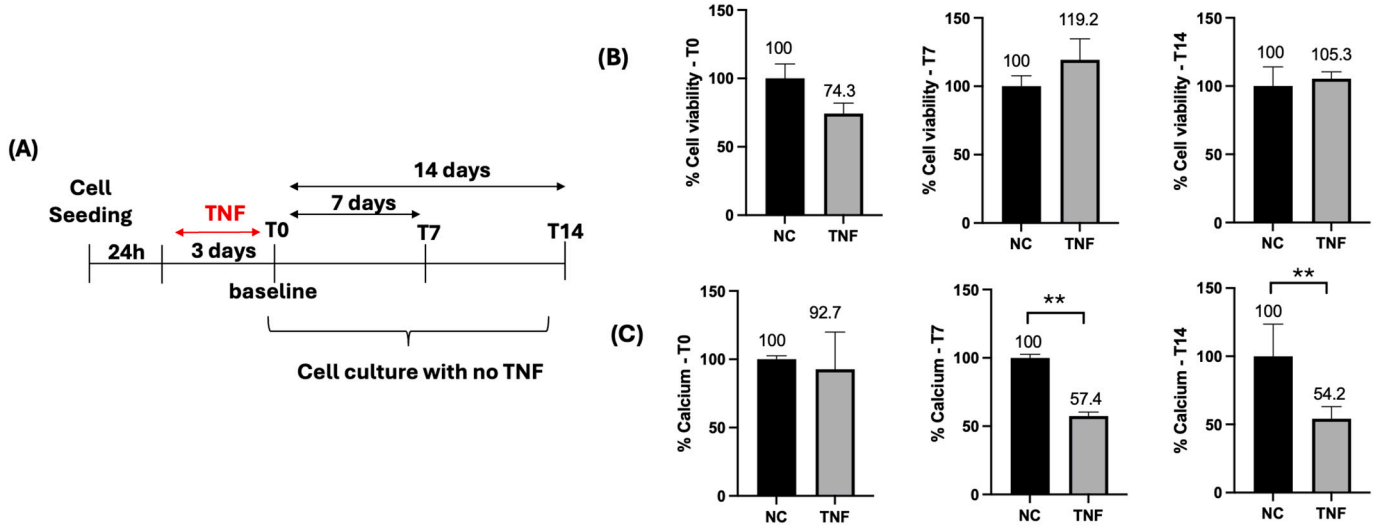

Fig. 1. Establishment of the inflammatory model. (A) Schematic representation of the experimental design. (B) Bar graph showing mean ± standard deviation of cell viability immediately after treatment (T0) and after 7 (T7) and 14 days (T14). (C) Calcium deposition assessed at 0 (T0), 7 (T7), and 14 days (T14). Data represent mean values, and [indicates statistically significant differences (**$p < 0.01$). Statistical analysis was performed using Student's *t*-test ($n = 6$).

described by our group [37,38]. Briefly, 2% chitosan (CH) solution was prepared by dissolving chitosan powder (310,000–375,000 Da; 75%–85% deacetylated, pH 3.5, Sigma-Aldrich) in 2% aqueous solution of acetic acid (Sigma-Aldrich) for 24 h. For CH-Ca (chitosan-calcium scaffolds) formulations, an aqueous suspension of $Ca(OH)_2$ at 1% *w/v* (pH 12.0, Sigma-Aldrich) was added to the chitosan solution (1:2) drop by drop under 1000 rpm stirring for 5 min. The CH and CH-Ca solutions were poured into Teflon molds and subjected to gradual freezing (−20 °C/−80 °C/−198 °C) and freeze-drying (Liotop L101, Liobras, São Carlos, São Paulo, Brazil) at −56 °C overnight. Using a biopsy punch (Kolplast ci LTDA.; Itupeva), scaffolds with 2 mm thickness and 6 mm in diameter were prepared. Then, the scaffolds were cross-linked in 25% glutaraldehyde (Sigma-Aldrich) vapor during 6 h. SV incorporation was performed by immersing CH and CH-Ca scaffolds for drug adsorption in sterile 1 μM simvastatin solution (1.5 μL/mm^2 for 72 h) prepared in PBS (phosphatebuffered saline; pH 7.4; GIBCO, Invitrogen, Carlsbad, CA, USA). The scaffolds were then incubated at 37 °C for 72 h and washed in PBS to eliminate non-adsorbed drug. Four experimental groups were stablished: chitosan (CH; control), chitosan–calcium (CH-Ca), chitosan–simvastatin (CH-SV), and chitosan–calcium–simvastatin (CH-Ca-SV). These scaffolds were previously characterized by Soares et al. [38].

For biological evaluations, scaffolds were disinfected in 70% ethanol under vacuum and rinsed three times in PBS. To obtain scaffold-conditioned media, samples were incubated in 500 μL complete DMEM at 37 °C and 5% CO_2 for up to 14 days [39]. SAOS-2 cells (2×10^4 cells/well) were seeded in 96-well plates and pre-stimulated with TNF-α (100 ng/mL) or control medium (serum-free) for 3 days. Cells were then cultured with scaffold extracts (200 μL), renewed every 24 h, for up to 14 days. The experimental design is demonstrated on Fig. 4A. Gene expression of TNF-α, MMP9 and IL-1β was assessed by real-time PCR ($n = 6$), 3 days after exposure to extracts. Cell viability (Alamar Blue assay; n = 6) was assessed at 1, 3, 7, and 14 days, to indirectly measure cell proliferation. The cells were incubated for 3 h at 37 °C and 5% CO_2 with Alamar Blue reagent (Life-Technologies, USA) diluted in serum-free DMEM (1:10) at each analysis period. After incubation, the supernatant was transferred to 96-well plates and analyzed in a fluorescence plate reader (540 nm excitation - 590 nm emission; Synergy Mx, BioTek, Winooski, USA). The data were normalized in comparison to the CH TNF- group, which was considered as 100% viability in each period. Osteogenic differentiation was evaluated through ALP activity (day 7; thymolphthalein monophosphate method; $n = 6$), mineralized matrix formation (day 14; Alizarin Red staining; n = 6), and gene expression of osteogenic markers BMP-2, OCN and OPN (day 14; real-time PCR; n = 6). For alizarin red, the wells were fixed in 70% ethanol and incubated in Alizarin Red solution (40 mM, pH 4.2; Sigma-Aldrich). Excess dye was removed with deionized water and 10% cetylpyridinium chloride solution was added to dissolve the mineral deposition. Absorbance was measured at 570 nm (Synergy Mx, BioTek, Winooski, USA). The data were normalized relative to the CH TNF- group, considered as having 100% mineralized matrix deposition.

2.4. In vivo analysis in calvaria defects with osteolytic lesion

The in vivo experiment was conducted using three-month-old male *Rattus norvegicus* albinus (Wistar strain) weighing 350–400 g. All procedures were approved by the Institutional Animal Care and Use Committee of the Araçatuba School of Dentistry, UNESP (FOA Process No. 0397-2020) and complied with the ARRIVE guidelines. A total of 60 animals ($n = 10$ per group per time point) were allocated based on previous studies using similar models, ensuring adequate statistical power ($\beta > 0.80$) to detect differences in bone formation. All animals were included in the analyses, with no exclusions or missing data. Based on the results of in vitro assays, only the scaffold formulations containing calcium and simvastatin at this bioactive dose (CH-Ca and CH-Ca-SV) were selected for in vivo evaluation. This strategy allowed us to focus on the most biologically relevant and translationally promising condition, while avoiding unnecessary animal use, in accordance with the principles of the 3Rs (Replacement, Reduction, and Refinement) and the guidelines of the Institutional Animal Care and Use Committee.

An inflammatory osteolytic model was established by local administration of TNF-α into the calvarial region, following an adaptation of the protocol by Kholy et al. [40]. Animals received three daily injections of 50 μL of TNF-α solution (0.02 ng/mL). After completion of the induction protocol, the animals underwent surgery to create the critical-size defect (Fig. 5A). General anesthesia was achieved with xylazine (6 mg/kg; Rompun®, Bayer, São Paulo, Brazil) and ketamine (70 mg/kg; Dopalen®, Agribands do Brasil Ltda., Paulínia, Brazil). Following trichotomy and antisepsis of the frontal region, a semilunar incision was made to expose the parietal bone. A 5-mm circular defect was created using a trephine bur (Neodent®, Curitiba, Brazil) mounted on an electric handpiece (Driller BLM 600 Plus®, Carapicuíba, Brazil), under continuous sterile saline irrigation. The dura mater was carefully preserved during osteotomy. Defects were then filled according to the experimental groups: blood clot (COAG group), CH-Ca scaffolds, or CH-Ca-SV

scaffolds. Only animals that developed the osteolytic lesion after TNF-α induction were used in the study. Soft tissues were repositioned and sutured to achieve primary closure (4-0 silk, Ethicon, São Paulo, Brazil). Postoperative care included a single intramuscular dose of penicillin G-benzathine (24,000 IU; Fort Dodge Animal Health Ltd., Campinas, Brazil).

Each experimental group was subdivided according to euthanasia time (7 and 30 days). Animals were euthanized via a lethal dose of sodium thiopental (150 mg/kg; Cristália Ltd., Itapira, Brazil). Calvarial samples were harvested immediately and fixed in 4% buffered formaldehyde for 48 h. Subsequently, samples were scanned by micro-computed tomography (SkyScan 1174; Bruker-microCT, Kontich, Belgium) using an X-ray source set at 50 kV. After micro-CT analysis, specimens were demineralized in 10% EDTA. Upon complete decalcification, tissues were processed and embedded in paraffin. Serial longitudinal sections (6 μm) were obtained and stained with hematoxylin–eosin (H&E) and Masson's Trichrome for histological evaluation.

Immunohistochemistry for TNF-α, IL-1β, OCN (osteocalcin) and OPN (osteopontin) was performed at both time-points. After deparaffinization in xylene and rehydration through a graded ethanol series (100°–100°–100°–90°–70° GL), antigen retrieval was performed by immersing the sections in Diva Decloaker® buffer (Biocare Medical, CA, USA) inside a pressurized Decloaking Chamber® at 95 °C for 10 min. All immunohistochemical steps included washes in 0.1 M PBS (pH 7.4). Endogenous peroxidase and nonspecific binding were blocked with 3% hydrogen peroxide for 1 h and 1% bovine serum albumin for 12 h, respectively. Sections were then incubated for 24 h with primary antibodies (Biorbyt Ltd., Cambridge, UK), diluted in Dako Antibody Diluent® (Dako Laboratories, CA, USA). The Universal Dako Labeled HRP Streptavidin–Biotin Kit® was used for detection, consisting of 2 h incubation with the biotinylated secondary antibody followed by 1 h incubation with HRP-conjugated streptavidin. Signal development was achieved using the DAB chromogen kit (Dako Laboratories). Sections were counterstained with hematoxylin, dehydrated in ascending alcohols, cleared in xylene, and mounted with coverslips. Negative controls were processed identically but without primary antibodies. A semi-quantitative analysis was performed using the following expanded criteria [41]: 0 – no immunolabeling (total absence of immunoreactive cells); 1 – low immunolabeling (1/4 of cells per area); 2 – moderate immunolabeling (1/2 of cells per area); 3 – high immunolabeling (3/4 of cells per area).

2.5. Statistical analysis

Two independent experiments were performed for all assays. Data were initially assessed for normality using the Shapiro–Wilk test and for homogeneity of variances using Levene's test. When parametric assumptions were met, comparisons between two groups were performed using Student's *t*-test, and comparisons among multiple groups were conducted using one- or two-way analysis of variance (ANOVA), as appropriate. Post hoc multiple comparisons were carried out using Tukey's test.

For semiquantitative immunohistochemical analyses based on ordinal scoring data, group comparisons were performed using the Newman–Keuls multiple comparisons test. A significance level of 5% was adopted for all analyses ($p < 0.05$).

3. Results

3.1. In vitro inflammatory model and SV-dosage selection

The results of the inflammatory model selection are presented in Fig. 1. No significant reduction in cell viability was observed at any time point following TNF-α exposure (Fig. 1B). However, calcium deposition decreased significantly by approximately 42.6% and 45.8% at 7 and 14 days, respectively (Fig. 1C). Regarding the dose–response effect of SV on SAOS-2 viability (Fig. 2), the concentrations of 10 and 5 μM simvastatin markedly reduced cell viability (Fig. 2A). Therefore, 1 μM SV was selected for the assessment of anti-inflammatory potential. Cells treated with 1 μM SV in the presence of TNF-α showed a significant reduction in TNF-α, IL-1β, and MMP9 gene expression compared with the TNF-α-only group, demonstrating an anti-inflammatory effect. However, TNF-α and MMP9 levels remained significantly higher than those of the negative control (Fig. 2B). Regarding the bioactive potential of the selected SV concentration (Fig. 3), 1 μM SV significantly increased ALP activity (Fig. 3A) and calcium deposition (Fig. 3B), whereas TNF-α markedly reduced these markers compared with the negative control. Cells treated with both TNF-α and SV exhibited a protective effect, with significantly higher ALP activity and calcium deposition than the TNF-α-only group. Furthermore, SV treatment significantly upregulated the expression of BMP-2, OCN, and OPN (Fig. 3C). However, no significant differences were observed between the TNF-α and SV_TNF groups compared with the negative control.

3.2. In vitro analyses of SV-loaded scaffolds

Alamar Blue assay data (Fig. 4B) showed significant no significant differences in cell viability among all groups at all time-points, regardless on the treatment with TNF-α. Gene expression analysis of inflammatory mediators (Fig. 4C) revealed that TNF-α treatment significantly increased TNF-α, MMP9 and IL-1β expression across all experimental groups. However, this increase was significantly lower in the CH TNF+ group compared to the CH-SV TNF+ and CH-Ca-SV TNF+ groups, indicating the anti-inflammatory effect of SV. Bioactivity analysis showed that ALP activity (Fig. 4D) was significantly enhanced only in the CH-Ca-SV group, in the absence of TNF, and in both the CH-SV and CH-Ca-SV groups in the presence of TNF, compared to CH. Alizarin Red staining (Fig. 4E) revealed a significant increase in mineralization for the CH-Ca-SV group pre-treated with TNF compared to CH TNF-. Mineralization nodules were larger and more well-defined in the CH-SV and CH-Ca groups compared to CH, both in the presence and absence of TNF. The CH-Ca-SV group exhibited more scattered nodules, with a slightly more pronounced pattern in cells pre-treated with TNF (Fig. 4F). Also, the CH-Ca-SV treatment showed the strongest promotion of osteogenic differentiation (Fig. 4G), significantly increasing BMP-2, OCN, and OPN expression, even under inflammatory conditions (TNF+). CH-Ca-SV demonstrated consistent superiority over other groups, suggesting potential for enhancing osteogenesis and addressing TNF-induced inhibition.

3.3. In vivo analysis of CH-Ca-SV scaffold in osteolytic bone lesions

Micro-computed tomography (micro-CT) analysis revealed clear differences in bone regeneration patterns among the experimental groups over time (Fig. 5B). At 7 days, all groups exhibited limited bone formation, predominantly restricted to the margins of the defect, with no significant differences in bone volume fraction. At 30 days, however, the CH-Ca-SV group demonstrated a marked increase in newly formed bone, characterized by more extensive bridging from the defect borders toward the central region. Quantitative micro-CT analysis confirmed that the CH-Ca-SV group presented a significantly higher bone volume fraction compared with both the COAG and CH-Ca groups at this later time point (Fig. 5C), indicating an accelerated and more effective regenerative response.

Histomorphometric analysis using Masson's trichrome staining further corroborated the micro-CT findings (Fig. 5D). At 7 days, all groups showed predominance of connective tissue within the defect area, with minimal bone formation limited to the peripheral regions. By 30 days, the CH-Ca-SV group exhibited a pronounced increase in bone tissue area concomitant with a significant reduction in connective tissue, resulting in the highest bone-to-connective tissue ratio among the

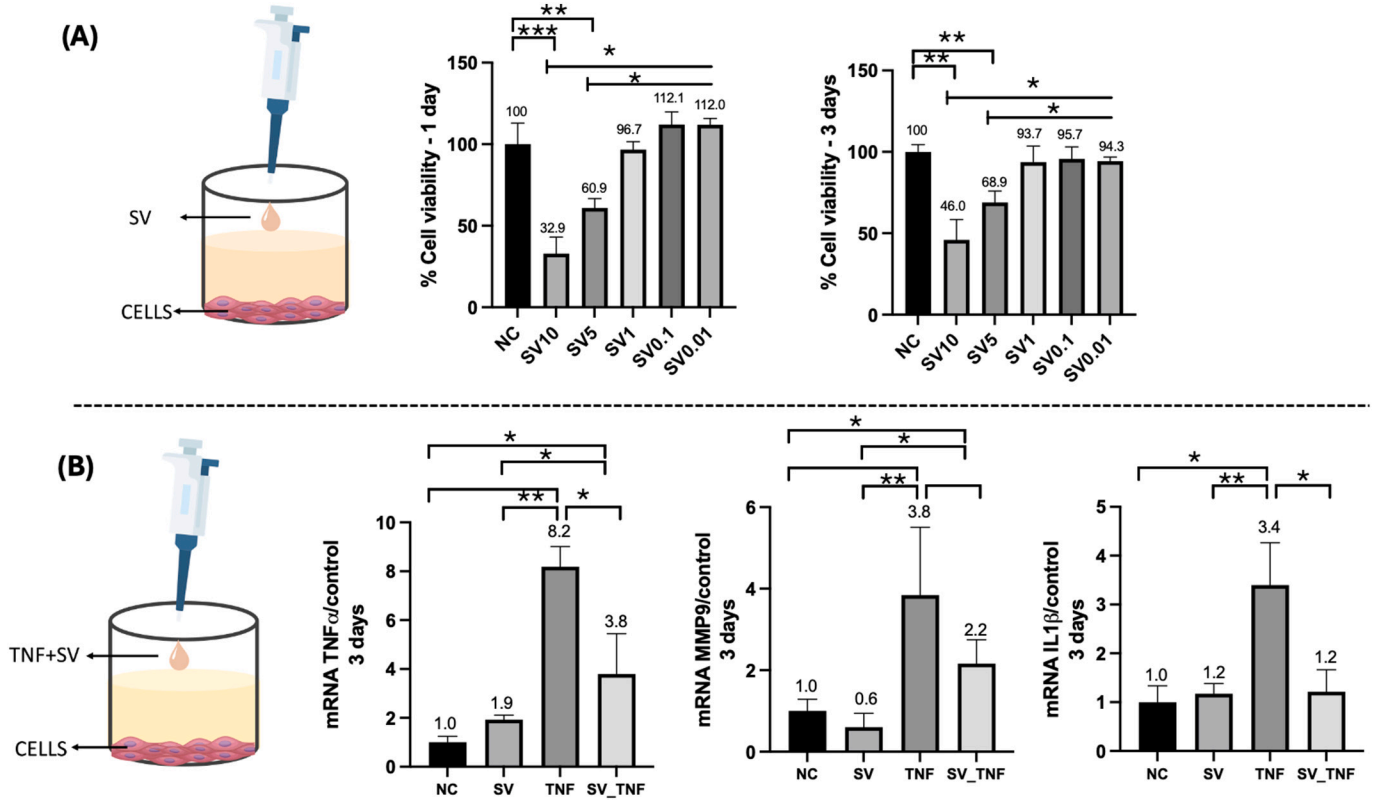

Fig. 2. (A) MTT assay evaluating the cytocompatibility of simvastatin (SV) at different concentrations. Bar graphs represent mean ± standard deviation of cell viability after 1 and 3 days of exposure. (B) Anti-inflammatory effects of SV under TNF-α stimulation. Relative gene expression levels of inflammatory markers were quantified by real-time PCR using TaqMan assays. Data represent mean values, and [indicates statistically significant differences (*$p < 0.05$; **$p < 0.01$). Data were analyzed using One-Way ANOVA followed by Tukey's test ($n = 6$).

groups (Fig. 5E). In contrast, the COAG group remained largely occupied by connective tissue at both time points, while the CH-Ca group displayed intermediate behavior, with partial bone formation and persistence of scaffold remnants within the defect.

Qualitative histological evaluation using H&E staining provided additional insight into the spatial organization and maturation of the newly formed tissue (Figs. 6 and 7). At 7 days, the COAG and CH-Ca groups exhibited bone neoformation confined to the defect margins, associated with a dense connective tissue matrix and evident inflammatory infiltrate. In the CH-Ca-SV group, although early bone formation was also primarily peripheral, the newly formed bone appeared more continuous and better organized, accompanied by a visibly reduced inflammatory infiltrate. At 30 days, bone formation in the COAG group remained limited, with the defect area still predominantly filled by connective tissue. The CH-Ca group showed discrete mineralization foci extending toward the central region; however, scaffold remnants were still evident, suggesting slower degradation and delayed tissue replacement. In contrast, the CH-Ca-SV group exhibited more extensive and continuous bone formation progressing from the margins toward the center of the defect, with greater central mineralization and improved tissue integration. Notably, the scaffold structure in this group remained identifiable but showed better integration with the newly formed bone, indicating a balance between scaffold stability and tissue remodeling.

Immunohistochemical analysis supported the histological observations regarding the inflammatory status of the defect area (Fig. 8). At 7 days, all groups displayed detectable TNF-α and IL-1β immunolabeling, consistent with the inflammatory nature of the osteolytic model. At 30 days, however, both the CH-Ca and CH-Ca-SV groups exhibited significantly reduced TNF-α and IL-1β immunostaining scores compared with the COAG group (Fig. 8A and C). Representative images (Fig. 8B and D) confirmed weaker and more localized immunolabeling in the scaffold-treated groups, particularly in the CH-Ca-SV group, indicating attenuation of the inflammatory response in parallel with enhanced bone regeneration.

To further characterize the regenerative profile of the scaffolds, immunohistochemical staining for the osteogenic markers osteocalcin (OCN) and osteopontin (OPN) was performed (Fig. 9). At 7 days, OCN and OPN immunolabeling was discrete and predominantly localized to the defect margins in all groups, consistent with early stages of bone healing. At 30 days, however, the CH-Ca-SV group exhibited significantly higher OCN and OPN immunostaining compared with the COAG and CH-Ca groups, with more intense and widespread labeling throughout the newly formed bone tissue. In contrast, the COAG group showed weak and sparse immunoreactivity, while the CH-Ca group presented intermediate levels of staining, mainly restricted to peripheral areas. These findings indicate enhanced osteogenic activity and matrix maturation in defects treated with the CH-Ca-SV scaffold, reinforcing its role in promoting bone regeneration under inflammatory conditions.

4. Discussion

The chitosan biomaterials incorporated with bioactive dosages of simvastatin (SV) have been proposed on the literature with exciting results for bone tissue engineering [42–45]. More recently, efforts have been made to develop SV delivery systems that could release smart SV dosages capable to modulate bone regeneration under inflammatory microenvironments. Mostly, the studies focus on the development of very sophisticated drug delivery systems [46–49]. In our previously work, we described the development of a low expensive chitosan-calcium-simvastatin (CH-Ca + SV) scaffold prepared with a very simple rout, capable to increase the bone regeneration in vitro and in vivo

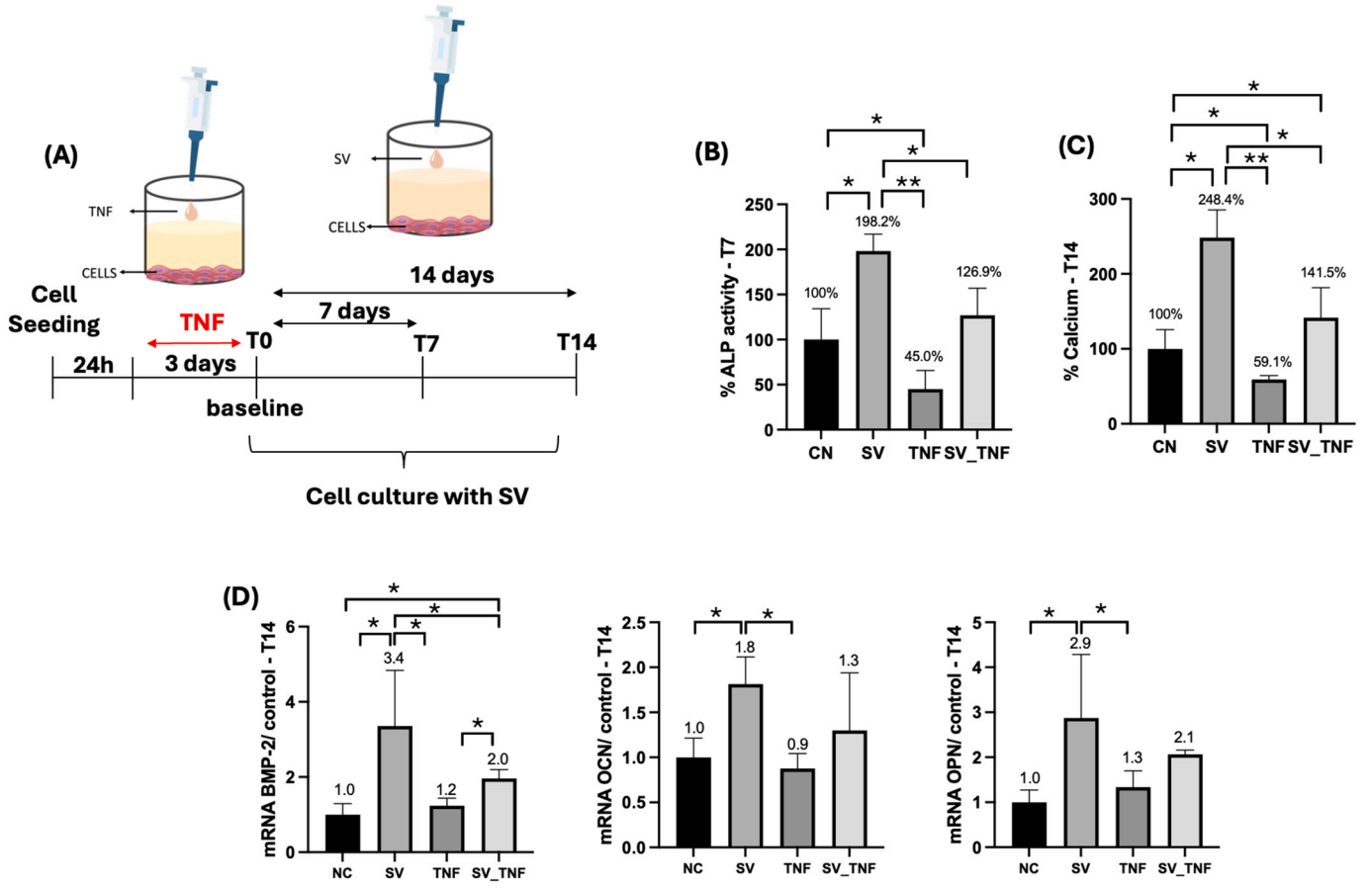

Fig. 3. Bioactive potential of SV under TNF stimulus. (A) Experimental design of simvastatin (1 μM) under an inflammatory environment. (B) Alkaline phosphatase (ALP) activity normalized to total protein content and expressed as a percentage relative to the control group (100%) after day 7 and 14. (C) Calcium deposition at 0, (d), 7 (e), 14 (f) days. (D) Relative mRNA expression of BMP-2, OCN, and OPN analyzed by real-time PCR. Values represent the mean, and [indicates statistically significant differences (*$p < 0.05$; **$p < 0.01$). Data were analyzed using One-Way ANOVA followed by Tukey's test ($n = 6$).

[22,38]. In the present investigation, we tested this scaffold as a multifunctional platform for bone regeneration, exploring bioactive and anti-inflammatory potentials of SV.

The CH–Ca scaffold originally developed by Soares et al. [37] exhibited a highly organized and interconnected macroporous architecture, with rounded pores, high overall porosity (86.9%), and a mean pore diameter of approximately 202 μm. These structural features were attributed to the combined effects of a controlled multi-step freezing regimen and a CO_2-mediated pore formation mechanism arising from the interaction between calcium hydroxide and acetic acid in the chitosan solution, called as bubbling-effect. Vapor-phase glutaraldehyde cross-linking effectively stabilized the chitosan matrix while preserving porosity and biocompatibility, resulting in enhanced structural integrity, controlled degradation, and sustained calcium release, key attributes for tissue-engineering applications. Building on this platform, simvastatin (SV) was incorporated into the pre-established CH–Ca scaffold by Soares et al. [38], to explore its potential as a cell-homing strategy, based on its previously reported pro-mineralization and chemotactic effects [36]. FTIR analysis indicated calcium complexation within the chitosan matrix, whereas SV interacted predominantly through weak hydrogen-bonding interactions, which directly influenced its release behavior. While calcium release remained controlled, SV exhibited a pronounced burst release within the first hours, reaching a peak at approximately 2 h.

The positive effect simvastatin-functionalized chitosan–calcium scaffold on SAOS-2 cells was also previously demonstrated by Gallinari et al. [22]. This study demonstrated superior biological performance compared with pure chitosan scaffolds, particularly with respect to porosity, cell viability, and osteogenic potential in SAOS-2 cells. The highly organized and interconnected macroporous architecture supported enhanced cell infiltration and increased cellular density in when cells were cultured onto scaffolds. Beyond its structural advantages, CH–Ca–SV exhibited the most pronounced bioestimulatory effect in both direct and indirect culture conditions, irrespective of osteogenic medium supplementation, indicating a synergistic interaction between the chitosan–calcium matrix and low-dose simvastatin. This synergy translated into enhanced osteoblastic differentiation, as evidenced by increased ALP activity and significantly greater mineralized matrix deposition. Notably, exposure to CH–Ca–SV extracts resulted in a marked increase in mineralized nodule formation at both early and later time points, reinforcing its capacity to actively promote osteogenesis. Collectively, these findings indicate that simvastatin functionalization substantially augments the bioactivity of the CH–Ca scaffold, supporting its potential as a promising platform for mineralized tissue regeneration.

Based on these properties, we hypothesized that simvastatin delivery in combination with a CH–Ca scaffold could establish a microenvironment favorable to osteogenic differentiation while attenuating inflammation in TNF-α–challenged SAOS-2 cells, thereby supporting bone regeneration. To simulate a pre-existing inflammatory condition in vitro, SAOS-2 cells were exposed to TNF-α (100 ng/mL) for 3 days, a protocol that markedly impaired mineralized matrix deposition without compromising cell viability. Cells were then preconditioned with TNF-α and subsequently cultured in scaffold-derived extracts, in the absence of continued TNF-α exposure, allowing evaluation of the ability of scaffold-released components to restore the regenerative potential of SAOS-2 cells following an inflammatory insult. In accordance with the

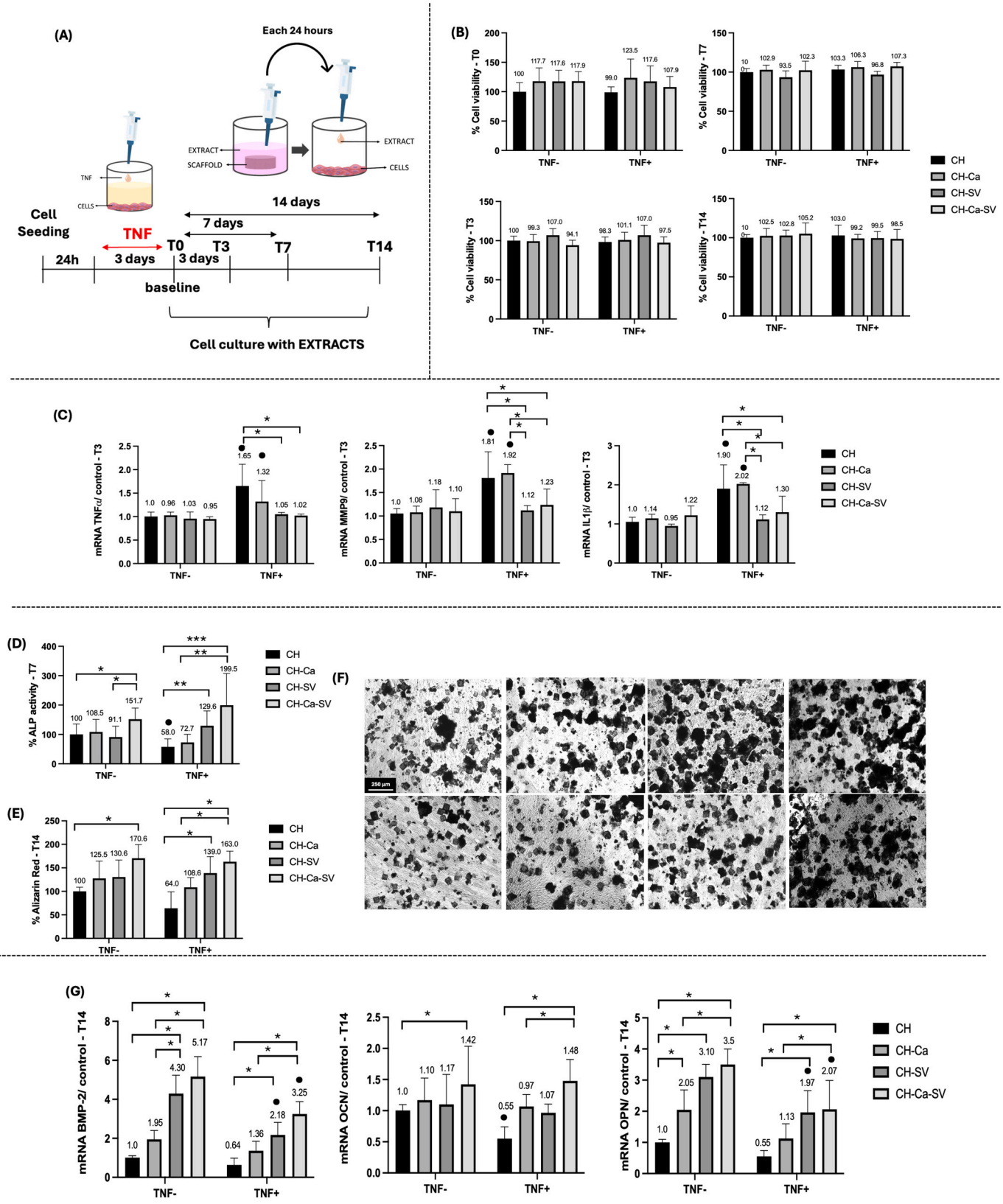

Fig. 4. In vitro evaluation of simvastatin-loaded scaffolds under inflammatory conditions. (A) Schematic representation of the experimental design. (B) Cell viability assessed using the Alamar Blue assay. (C) Quantitative analysis of pro-inflammatory gene expression (TNF-α, MMP9, IL-1β) by RT-qPCR. (D) Alkaline phosphatase (ALP) activity. (E) Calcium deposition evaluated by Alizarin Red staining. (F) Representative images of mineralized nodule formation (white arrows indicate the nodules) of data on (E). (G) Expression of osteogenic genes (BMP-2, OCN, OPN) assessed by RT-qPCR. Values represent the mean, and [indicates statistically significant differences among groups at each time-point. ●indicates significant differences between time-points for each group (*$p < 0.05$; **$p < 0.01$; *** $p < 0.001$). Data were analyzed using the Two-Way ANOVA and Tukey's test, with a significance level of 5% ($n = 6$).

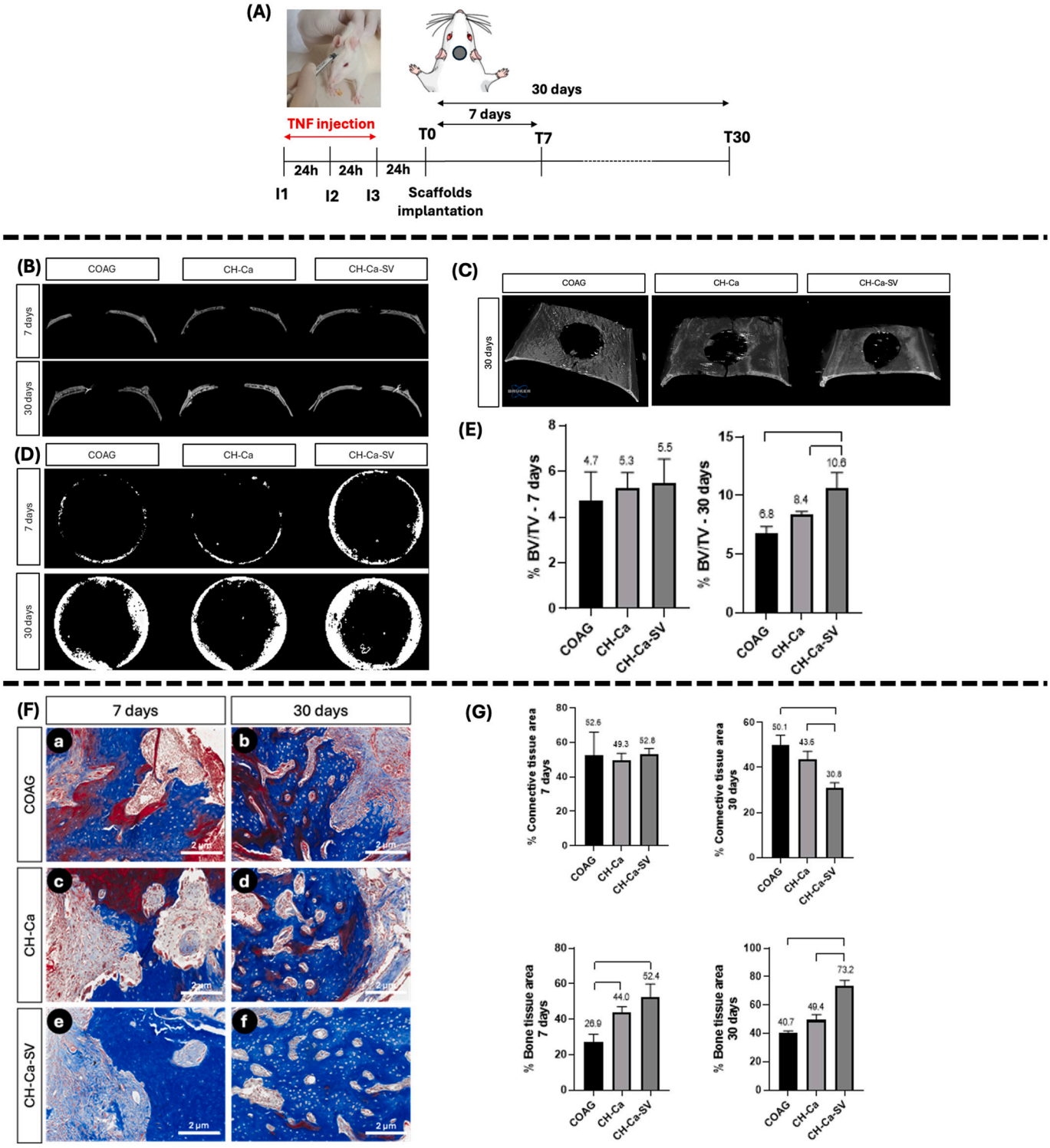

Fig. 5. In vivo experiments. (A) Experimental scheme showing induction of inflammatory in rats by TNF injection before calvaria defect. (B) Representative coronal micro-CT sections of the calvarial defects at 7 and 30 days for the COAG, CH-Ca, and CH-Ca-SV groups. (C) Three-dimensional micro-CT reconstructions of the same region of interest at 30 days, illustrating the spatial distribution of newly formed bone within the defect area. (D) Representative dorsal (top-view) micro-CT reconstructions of the calvarial defects at 7 and 30 days for the different experimental groups. (E) Quantitative analysis of bone volume fraction (BV/TV, %) obtained by micro-CT at 7 and 30 days. Data are presented as mean ± standard deviation. Brackets indicate statistically significant differences among groups at each time point ($p < 0.05$). (F) Masson's trichrome staining. Representative images of the experimental groups at 7 and 30 days. (G) Tissue percentage analysis by Masson's trichrome staining. Bar graphs showing the percentage of connective tissue and bone tissue at 7 and 30 days (one-way ANOVA; Tukey's post hoc test; * $p < 0.05$; $n = 10$). White arrows indicate the.

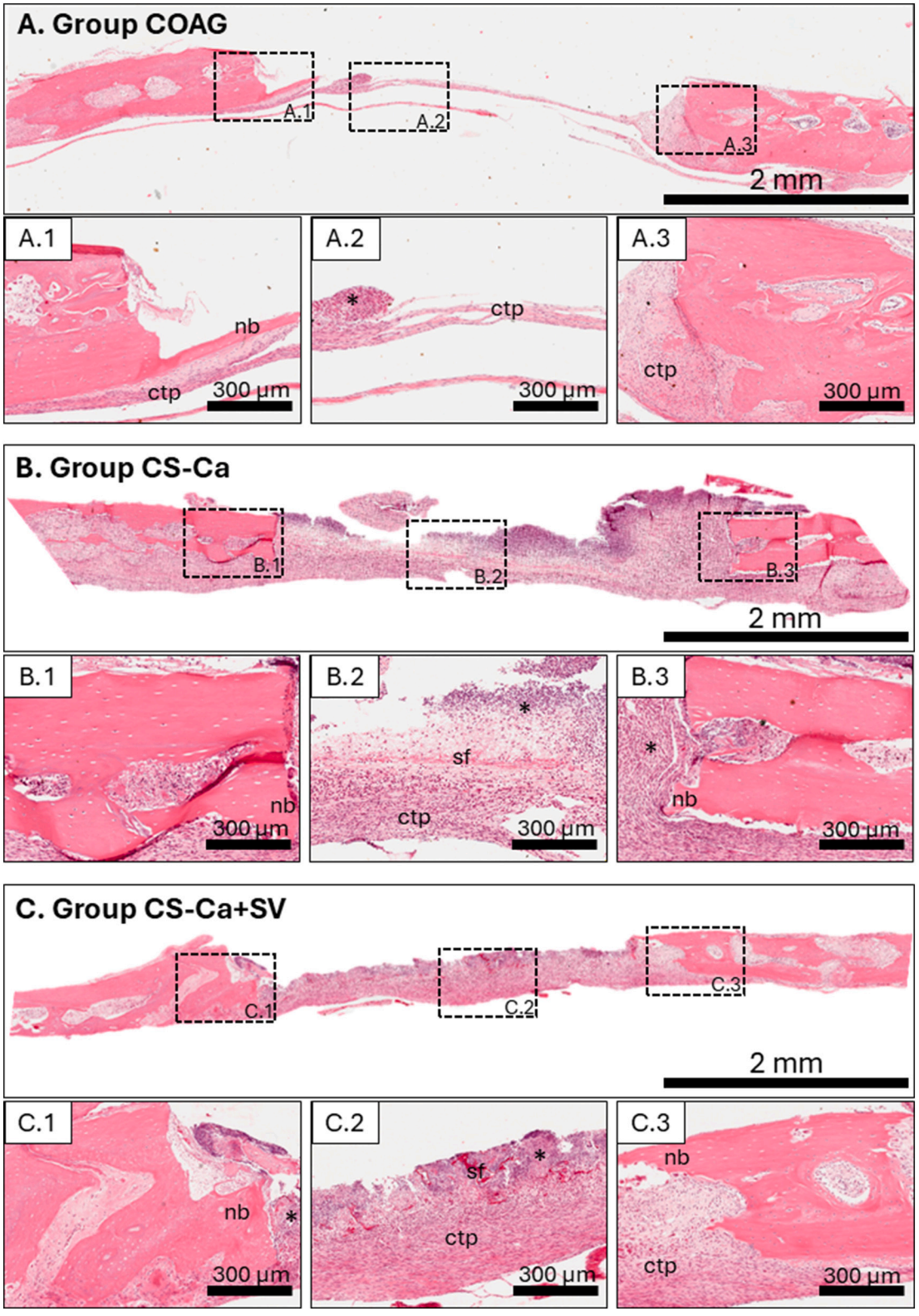

Fig. 6. H&E staining of in vivo samples collected after 7 days, showing the histological features of the tissues within the critical-sized defects. Photomicrographs of the COAG (A–A.3), CH-Ca (B—B.3), and CH-Ca + SV (C—B.3) groups. CH-Ca, chitosan-calcium hydroxide; ctp, connective tissue proper; nb, new bone; sf, scaffold; SV, simvastatin; *, inflammatory infiltrate.

literature emphasizing the potential of statins to modulate essential processes such as osteogenic differentiation and inflammation [11,13,14,22,50,51], the data obtained showed that the incorporation of SV into scaffolds not only preserved cellular functionality in TNF-α-mediated pro-inflammatory environments, but also promoted tissue regeneration at multiple scales.

Regarding the higher concentrations of SV (10 and 5 μM), a significant reduction in cell viability was observed, confirming previous

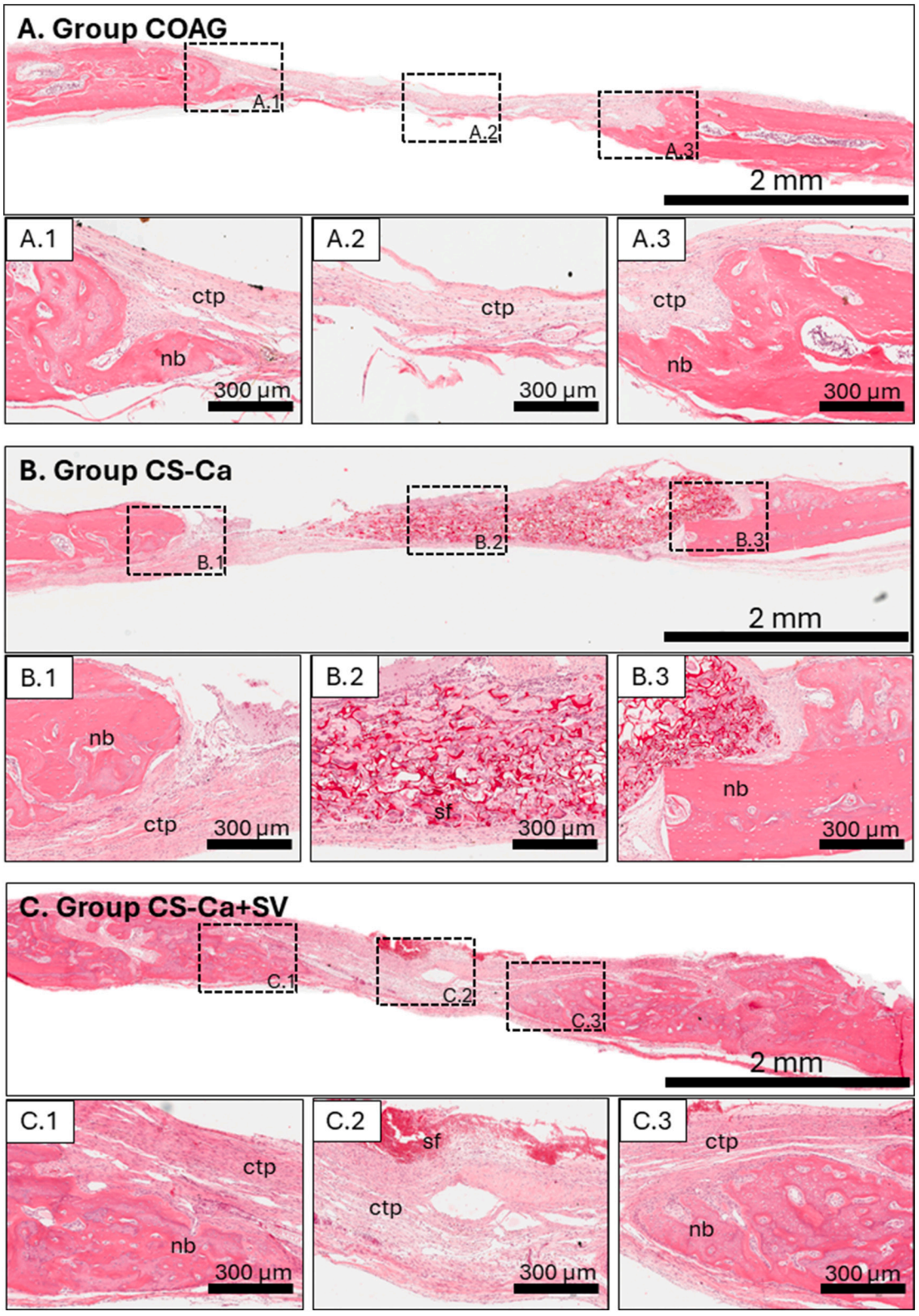

Fig. 7. H&E staining of in vivo samples collected after 30 days, showing the histological features of the tissues within the critical-sized defects. Photomicrographs of the COAG (A–A.3), CH-Ca (B—B.3), and CH-Ca + SV (C—B.3) groups. CH-Ca, chitosan-calcium hydroxide; ctp, connective tissue proper; nb, new bone; sf, scaffold; SV, simvastatin; *, inflammatory infiltrate.

studies reporting cytotoxic effects at higher doses [6,8,13,51,52]. In contrast, the concentration of 1 μM proved to be effective and not cytotoxic [22,36,38], preserving the viability of SAOS-2 cells and significantly reducing the expression of the pro-inflammatory genes TNF-α, IL-1β, and MMP9 in the presence of TNF-α. Although these levels remained higher than those of the negative control, the results suggest an anti-inflammatory effect. The pleiotropic effects of simvastatin on bone cells under TNF-α–mediated pro-inflammatory conditions have

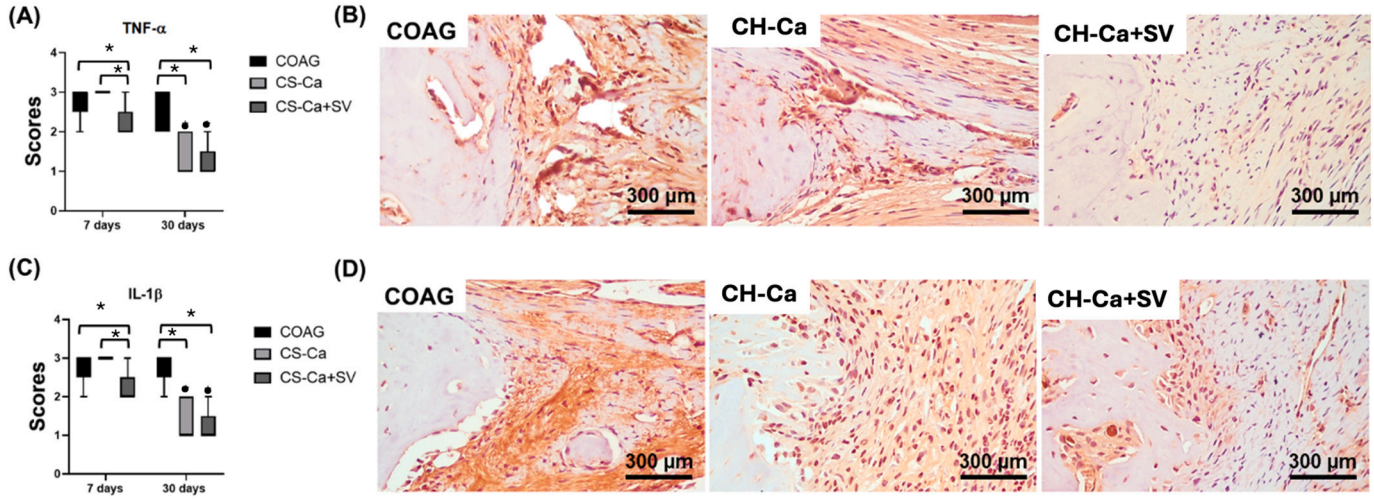

Fig. 8. Inflammatory immunohistochemistry analysis. (A) Bar graph of TNF-α immunostaining scores at 7 and 30 days. (B) Representative TNF-α immunostaining images for each experimental group at 30 days. (C) Bar graph of IL-1β immunostaining scores at 7 and 30 days. (D) Representative IL-1β immunostaining images for each experimental group at 30 days. Values represent the mean. [indicate statistically significant differences among groups at each time point, and * indicate statistically significant differences between time points within each group ($p < 0.05$). Data were analyzed using the Newman–Keuls multiple comparisons test ($n = 10$).

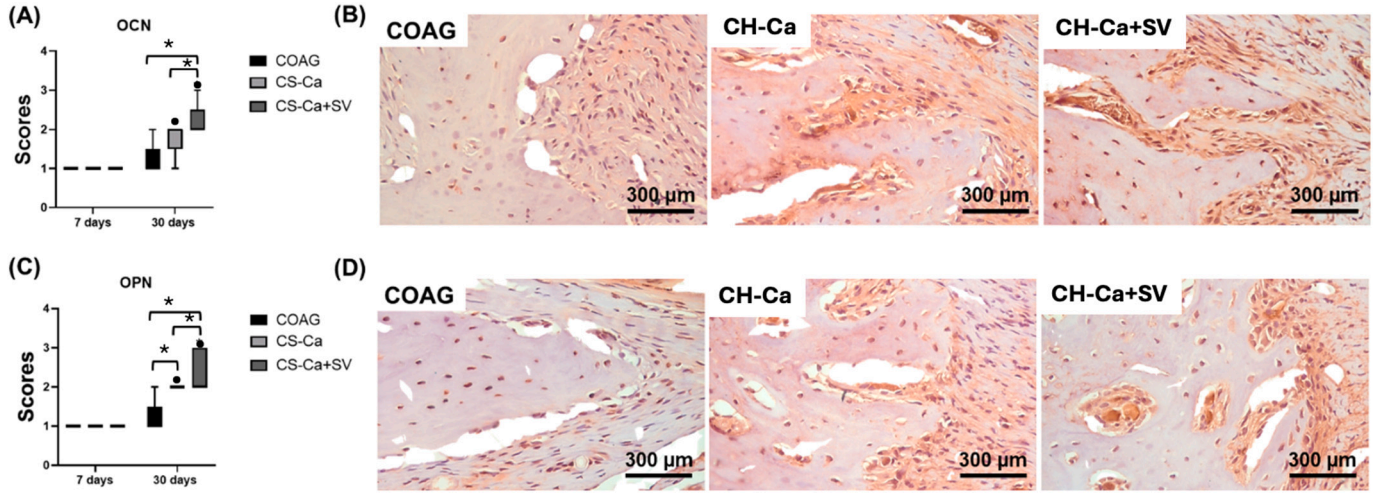

Fig. 9. Osteogenic immunohistochemistry analysis. (A) Bar graph of osteocalcin (OCN) immunostaining scores at 7 and 30 days. (B) Representative OCN immunostaining images for each experimental group at 30 days. (C) Bar graph of osteopontin (OPN) immunostaining scores at 7 and 30 days. (D) Representative OPN immunostaining images for each experimental group at 30 days. Values represent the mean. [indicate statistically significant differences among groups at each time point, and * indicate statistically significant differences between time points within each group ($p < 0.05$). Data were analyzed using the Newman–Keuls multiple comparisons test ($n = 10$).

been previously described in a classical study [53]. TNF-α suppresses BMP-2–induced osteogenic markers, including Runx2 and ALP activity, and simvastatin effectively reverses these inhibitory effects. Mechanistically, simvastatin restores BMP-Smad signaling by reversing TNF-α–mediated inhibition of Smad1/5/8 phosphorylation, while simultaneously suppressing TNF-α–induced activation of the Ras/Rho–MAPK pathway, including ERK1/2 and SAPK/JNK, through inhibition of Ras and RhoA membrane localization. The involvement of mevalonate intermediates was confirmed, as farnesyl pyrophosphate (FPP) and geranylgeranyl pyrophosphate (GGPP) abrogated simvastatin's effects, indicating dependence on Ras and RhoA prenylation. Simvastatin also reduced TNFR1 and TNFR2 mRNA levels, further decreasing cellular sensitivity to TNF-α.

In terms of osteogenesis, the 1 μM concentration of SV was sufficient to induce alkaline phosphatase (ALP) activity, stimulate calcium deposition and up-regulate the expression of the osteoblast markers BMP-2, OCN and OPN, also in conditions of inflammatory stress. These effects indicate a protective role of SV on the osteoblastic phenotype [10,11]. Accumulating evidence indicates that simvastatin, at concentrations ranging from 0.01 to 1 μM, promotes osteoblastic differentiation primarily through activation of the ERK1/2 signaling pathway, via mechanisms that appear largely independent of the mevalonate pathway [10,54–56]. Experimental studies have shown that simvastatin activates small GTPases such as Ras and RhoA, leading to ERK1/2 phosphorylation and subsequent upregulation of key osteogenic transcriptional regulators, including RUNX2 and BMP-2. This signaling cascade ultimately drives the commitment of mesenchymal progenitors toward an osteogenic phenotype. In addition, ERK1/2 activation has been reported to precede Smad1 phosphorylation, supporting a model in which simvastatin-induced BMP-2 expression acts in an autocrine or paracrine manner to sustain and amplify osteogenic signaling. Collectively, these findings delineate a coordinated Ras/RhoA–ERK1/2–BMP-2–Smad axis

as a central mechanism underlying the pro-osteogenic effects of simvastatin. In the present study, 1 μM simvastatin similarly upregulated BMP-2 gene expression in both TNF-α–stimulated and unstimulated cells, including when adsorbed onto CH–Ca scaffolds. This upregulation was accompanied by increased expression of osteocalcin (OCP) and osteopontin (OPN), which likely contributed to the observed enhancement of ALP activity and mineralized matrix deposition. Collectively, these findings indicate that simvastatin promotes BMP-induced osteoblastic differentiation under inflammatory conditions by simultaneously antagonizing TNF-α–Ras/Rho/MAPK signaling and enhancing BMP-Smad pathways, highlighting its therapeutic potential in mitigating inflammation-associated bone damage.

The bioactivity of SV under inflammatory conditions was preserved when incorporated into chitosan-based scaffolds, either in the pure formulation or in combination with calcium (CH-Ca). Incorporating chitosan into the carrier material provides additional anti-inflammatory and osteoinductive benefits [57]. Moreover, CH-Ca-SV scaffolds were effective in reducing the expression of pro-inflammatory genes and enhancing cell viability, suggesting that the controlled release of SV plays a key role in counteracting the deleterious effects of TNF-α. These effects are consistent with the reported ability of chitosan to modulate inflammatory mediators and support osteogenic commitment [57]. At the same time, these formulations also promoted osteoblastic differentiation, with the CH-Ca-SV group showing the most pronounced effects, including increased ALP activity, greater deposition of mineralized matrix and morphological evidence of differentiation. The superior performance of CH-Ca-SV scaffolds likely arises from the synergistic action of calcium, which favors mineral nucleation, and simvastatin, which activates osteogenic pathways, within a bioactive chitosan matrix [25].

Corroborating the in vitro results, the in vivo experiments confirmed that the CH-Ca-SV scaffold significantly enhanced bone regeneration in a critical-sized defect model under inflammatory conditions. Micro-CT and histological analyses showed a significant increase in new bone formation associated with organized collagen fiber deposition and absence of necrotic areas, indicating a favorable regenerative microenvironment. Detailed histopathological evaluation revealed that although the COAG and CH-Ca groups exhibited bone neoformation predominantly confined to the defect margins, the CH-Ca-SV group promoted more extensive and continuous bone formation progressing to the defect center, showing more pronounced mineralization. Furthermore, a pronounced reduction in inflammatory infiltrate was observed in the CH-Ca-SV group, especially at early time points, suggesting an immunomodulatory effect probably mediated by the reported anti-inflammatory properties of simvastatin [58,59]. This anti-inflammatory profile was accompanied by a significant increase in the expression of osteogenic markers, as demonstrated by the higher immunohistochemical labeling of OCN and OPN in the CH-Ca-SV group at 30 days, indicating enhanced osteoblastic activity, extracellular matrix maturation, and bone remodeling. Quantitative analysis using Masson's trichrome staining confirmed these findings, showing a significantly higher percentage of bone tissue and a concomitant reduction in connective tissue in the CH-Ca-SV group at both 7 and 30 days. These findings demonstrate that the combination of chitosan, calcium, and simvastatin creates a biomimetic environment that not only promotes osteogenesis [22,36], but also attenuates the inflammatory response, thereby accelerating and improving bone repair.

Recent clinical evidence further supports the anti-inflammatory and pro-osteogenic potential of simvastatin-based strategies, corroborating the biological effects observed in our in vitro and in vivo models. In cases of delayed tooth reimplantation, the adjunctive use of simvastatin in combination with platelet-rich fibrin and hydroxyapatite was associated with effective control of post-traumatic inflammation, prevention of inflammatory root and bone resorption, and promotion of periradicular bone formation [60]. Similarly, in a controlled clinical study involving immediate implant placement, simvastatin-treated patients exhibited significantly greater reductions in probing depth and bleeding on probing, along with superior preservation of crestal bone levels, compared with control subjects [61]. Collectively, these clinical outcomes are consistent with simvastatin's ability to modulate inflammatory responses while simultaneously enhancing osteogenic activity, reinforcing the translational relevance of its pleiotropic effects and demonstrating that the biological mechanisms identified in experimental models are also operative in human clinical settings.

In conclusion, the results of this study indicate that chitosan-based scaffolds with calcium and simvastatin represent a promising therapeutic approach for tissue engineering applications involving mineralized tissues under inflammatory conditions. The ability to modulate inflammation, promote osteogenesis, and preserve endothelial integrity suggests that this formulation could be valuable, specifically for the treatment of chronic lesions in regions such as the oral cavity. Despite these promising findings, the present study is limited by the absence of protein-level analyses, including ELISA-based quantification of inflammatory cytokines and direct assessment of osteogenic marker expression, which would further strengthen the mechanistic interpretation of the results. Future investigations should focus on elucidating the release kinetics of simvastatin and testing our results in more clinic relevant models, in order to support the translational potential of these biomaterials.

CRediT authorship contribution statement

Marjorie de Oliveira Gallinari: Writing – original draft, Visualization, Methodology, Investigation, Formal analysis, Data curation, Conceptualization. **Ester Alves Ferreira Bordini:** Validation, Methodology, Investigation, Formal analysis. **Elisa Mara de Abreu Furquim:** Methodology, Data curation. **Priscila Toninatto Alves de Toledo:** Writing – original draft, Visualization, Investigation, Formal analysis. **Vitor de Toledo Stuani:** Writing – original draft, Software, Investigation. **Ruan Henrique Delmonica Barra:** Investigation, Data curation. **Edilson Ervolino:** Validation, Resources, Methodology. **Luciano Tavares Angelo Cintra:** Writing – review & editing, Validation, Resources, Funding acquisition. **Carlos Alberto de Souza Costa:** Writing – review & editing, Supervision, Resources, Funding acquisition, Conceptualization. **Juliano Milanezi de Almeida:** Writing – review & editing, Visualization, Software. **Diana Gabriela Soares:** Writing – review & editing, Writing – original draft, Supervision, Project administration, Methodology, Funding acquisition, Conceptualization.

Declaration of Generative AI and AI-assisted technologies in the writing process

During the preparation of this work, the author(s) used ChatGPT (OpenAI) in order to assist with text refinement and clarity. After using this tool, the author(s) reviewed and edited the content as needed and take full responsibility for the content of the published article.

Declaration of competing interest

The authors declare that they have no known competing financial interests or personal relationships that could have appeared to influence the work reported in this manuscript.

Acknowledgments

The authors acknowledge and express their gratitude for the support provided by the São Paulo Research Foundation (FAPESP) [grant numbers 2016/15674-5, 2019/00020-8] and Coordination for the Improvement of Higher Education Personnel (CAPES) [Finance Code 001].

Appendix A. Supplementary data

Supplementary data to this article can be found online at https://doi.org/10.1016/j.ijbiomac.2026.151039.

Data availability

Data will be made available on request.

References

[1] J.S. Colombo, A.N. Moore, J.D. Hartgerink, R.N. D'Souza, Scaffolds to control inflammation and facilitate dental pulp regeneration, J Endod 40 (2014) S6–S12.
[2] R.A. Hortensius, B.A. Harley, Naturally derived biomaterials for addressing inflammation in tissue regeneration, Exp. Biol. Med. (Maywood) 241 (2016) 1015–1024.
[3] J.K. Liao, U. Laufs, Pleiotropic effects of statins, Annu. Rev. Pharmacol. Toxicol. 45 (2005) 89–118.
[4] J. Montero, G. Manzano, A. Albaladejo, The role of topical simvastatin on bone regeneration: A systematic review, J Clin Exp Dent 6 (2014) e286–e290.
[5] A. Oryan, A. Kamali, A. Moshiri, Potential mechanisms and applications of statins on osteogenesis: current modalities, conflicts and future directions, J. Control. Release 215 (2015) 12–24.
[6] Y. Okamoto, W. Sonoyama, M. Ono, K. Akiyama, T. Fujisawa, M. Oshima, Y. Tsuchimoto, Y. Matsuka, T. Yasuda, S. Shi, T. Kuboki, Simvastatin induces the odontogenic differentiation of human dental pulp stem cells in vitro and in vivo, J Endod 35 (2009) 367–372.
[7] Y. Shen, H. Wu, C. Wang, H. Shao, H. Huang, H. Jing, D. Li, Simvastatin attenuates cardiopulmonary bypass-induced myocardial inflammatory injury in rats by activating peroxisome proliferator-activated receptor γ, Eur. J. Pharmacol. 649 (2010) 255–262.
[8] K.S. Min, Y.M. Lee, S.O. Hong, E.C. Kim, Simvastatin promotes odontoblastic differentiation and expression of angiogenic factors via heme oxygenase-1 in primary cultured human dental pulp cells, J Endod 36 (2010) 447–452.
[9] S.Y. Lee, K.S. Min, G.W. Choi, J.H. Park, S.H. Park, S.I. Lee, E.C. Kim, Effects of simvastatin and enamel matrix derivative on Portland cement with bismuth oxide-induced growth and odontoblastic differentiation in human dental pulp cells, J Endod 38 (2012) 405–410.
[10] I.C. Tai, Y.H. Wang, C.H. Chen, S.C. Chuang, J.K. Chang, M.L. Ho, Simvastatin enhances rho/actin/cell rigidity pathway contributing to mesenchymal stem cells' osteogenic differentiation, Int. J. Nanomedicine 10 (2015) 5881–5894.
[11] S. Gupta, M. Del Fabbro, J. Chang, The impact of simvastatin intervention on the healing of bone, soft tissue, and TMJ cartilage in dentistry: a systematic review and meta-analysis, Int. J. Implant. Dent. 5 (2019) 17.
[12] K.S. Ahn, G. Sethi, M.M. Chaturvedi, B.B. Aggarwal, Simvastatin, a 3-hydroxy-3-methylglutaryl coenzyme A reductase inhibitor, suppresses osteoclastogenesis induced by receptor activator of nuclear factor-κB ligand through modulation of the NF-κB pathway, Int. J. Cancer 123 (2008) 1733–1740.
[13] X.Y. Zhu, E. Daghini, A.R. Chade, R. Lavi, C. Napoli, A. Lerman, L.O. Lerman, Disparate effects of simvastatin on angiogenesis during hypoxia and inflammation, Life Sci. 83 (2008) 801–809.
[14] A. Bitto, L. Minutoli, D. Altavilla, F. Polito, T. Fiumara, H. Marini, M. Galeano, M. Calò, P. Lo Cascio, M. Bonaiuto, A. Migliorato, A.P. Caputi, F. Squadrito, Simvastatin enhances VEGF production and ameliorates impaired wound healing in experimental diabetes, Pharmacol. Res. 57 (2008) 159–169.
[15] H. Wu, H. Jiang, D. Lu, C. Qu, Y. Xiong, D. Zhou, M. Chopp, A. Mahmood, Induction of angiogenesis and modulation of vascular endothelial growth factor receptor-2 by simvastatin after traumatic brain injury, Neurosurgery 68 (2011) 1363–1371.
[16] D. Falcone, L. Gallelli, A. Di Virgilio, L. Tucci, M. Scaramuzzino, R. Terracciano, G. Pelaia, R. Savino, Effects of simvastatin and rosuvastatin on RAS protein, matrix metalloproteinases and NF-κB in lung cancer and in normal pulmonary tissues, Cell Prolif. 46 (2013) 172–182.
[17] P.C. Chang, L.Y. Chong, A.S. Dovban, L.P. Lim, J.C. Lim, M.Y. Kuo, C.H. Wang, Sequential platelet-derived growth factor–simvastatin release promotes dentoalveolar regeneration, Tissue Eng. Part A 20 (2014) 356–364.
[18] Y.J. Chen, L.S. Chang, Simvastatin induces NFκB/p65 down-regulation and JNK1/c-Jun/ATF-2 activation, leading to matrix metalloproteinase-9 (MMP-9) but not MMP-2 down-regulation in human leukemia cells, Biochem. Pharmacol. 92 (2014) 530–543.
[19] J. Tan, N. Yang, X. Fu, Y. Cui, Q. Guo, T. Ma, X. Yin, H. Leng, C. Song, Single-dose local simvastatin injection improves implant fixation via increased angiogenesis and bone formation in an ovariectomized rat model, Med. Sci. Monit. 21 (2015) 1428–1439.
[20] S. Maeno, Y. Niki, H. Matsumoto, H. Morioka, T. Yatabe, A. Funayama, Y. Toyama, T. Taguchi, J. Tanaka, The effect of calcium ion concentration on osteoblast viability, proliferation and differentiation in monolayer and 3D culture, Biomaterials 26 (2005) 4847–4855.
[21] J.C. García-Perdiguero, N. Gómez-Cerezo, M. Gisbert-Garzarán, M. Manzano, M. Vallet-Regí, Unraveling the role of calcium in the osteogenic behavior of mesoporous bioactive glass nanoparticles, Acta Biomater. 198 (2025) 482–496.
[22] M.O. Gallinari, E.A.F. Bordini, V.T. Stuani, F.B. Cassiano, C.C.D.S.B. Melo, J. M. Almeida, L.T.A. Cintra, C.A. De Souza Costa, D.G. Soares, Assessment of the regenerative potential of macro-porous chitosan–calcium simvastatin scaffolds on bone cells, Braz. Oral Res. 37 (2023) e018.
[23] T. Tanigo, R. Takaoka, Y. Tabata, Sustained release of water-insoluble simvastatin from biodegradable hydrogel augments bone regeneration, J. Control. Release 143 (2010) 201–206.
[24] M.S. Bae, D.H. Yang, J.B. Lee, D.N. Heo, Y.D. Kwon, I.C. Youn, K. Choi, J.H. Hong, G.T. Kim, Y.S. Choi, E.H. Hwang, I.K. Kwon, Photo-cured hyaluronic acid-based hydrogels containing simvastatin as a bone tissue regeneration scaffold, Biomaterials 32 (2011) 8161–8171.
[25] T. Fukui, M. Ii, T. Shoji, T. Matsumoto, Y. Mifune, Y. Kawakami, H. Akimaru, A. Kawamoto, T. Kuroda, T. Saito, Y. Tabata, R. Kuroda, M. Kurosaka, T. Asahara, Therapeutic effect of local administration of low-dose simvastatin-conjugated gelatin hydrogel for fracture healing, J. Bone Miner. Res. 27 (2012) 1118–1131.
[26] I.C. Tai, Y.C. Fu, C.K. Wang, J.K. Chang, M.L. Ho, Local delivery of controlled-release simvastatin/PLGA/HAp microspheres enhances bone repair, Int. J. Nanomedicine 8 (2013) 3895–3904.
[27] Y. Naito, T. Terukina, S. Galli, Y. Kozai, S. Vandeweghe, T. Tagami, T. Ozeki, T. Ichikawa, P.G. Coelho, R. Jimbo, The effect of simvastatin-loaded polymeric microspheres in a critical-size bone defect in the rabbit calvaria, Int. J. Pharm. 461 (2014) 157–162.
[28] S.D. Nath, N.T. Linh, A. Sadiasa, B.T. Lee, Encapsulation of simvastatin in PLGA microspheres loaded into hydrogel-loaded BCP porous spongy scaffold as a controlled drug delivery system for bone tissue regeneration, J. Biomater. Appl. 28 (2014) 1151–1163.
[29] A. Miyazawa, T. Matsuno, K. Asano, Y. Tabata, T. Satoh, Controlled release of simvastatin from biodegradable hydrogels promotes odontoblastic differentiation, Dent. Mater. J. 34 (2015) 466–474.
[30] A. Moshiri, M. Shahrezaee, B. Shekarchi, A. Oryan, K. Azma, Three-dimensional porous Gelapin–simvastatin scaffolds promoted bone defect healing in rabbits, Calcif. Tissue Int. 96 (2015) 552–564.
[31] X.Z. Yan, J.J. van den Beucken, X. Cai, N. Yu, J.A. Jansen, F. Yang, Periodontal tissue regeneration using enzymatically solidified chitosan hydrogels with or without cell loading, Tissue Eng. Part A 21 (2015) 1066–1076.
[32] P. Gentile, V.K. Nandagiri, J. Daly, V. Chiono, C. Mattu, C. Tonda-Turo, G. Ciardelli, Z. Ramtoola, Localised controlled release of simvastatin from porous chitosan–gelatin scaffolds engrafted with simvastatin-loaded PLGA microparticles for bone tissue engineering application, Mater. Sci. Eng. C 59 (2016) 249–257.
[33] N. Asl Aminabadi, E. Maljaei, L. Erfanparast, A. Ala Aghbali, H. Hamishehkar, E. Najafpour, Simvastatin versus calcium hydroxide direct pulp capping of human primary molars: a randomized clinical trial, J. Dent. Res. Dent. Clin. Dent. Prospects 7 (2013) 8–14.
[34] N. Asl Aminabadi, S. Satrab, E. Najafpour, M. Samiei, Z. Jamali, S. Shirazi, A randomized trial of direct pulp capping in primary molars using MTA compared to 3Mixtatin: a novel pulp capping biomaterial, Tissue Eng. Part A 20 (2014) 356–364.
[35] D.G. Soares, Z. Zhang, F. Mohamed, T.W. Eyster, C.A. de Souza Costa, P.X. Ma, Simvastatin and nanofibrous poly(L-lactic acid) scaffolds to promote the odontogenic potential of dental pulp cells in an inflammatory environment, Acta Biomater. 68 (2018) 190–203.
[36] D.G. Soares, G. Anovazzi, E.A.F. Bordini, U.O. Zuta, M.L.A. Silva Leite, F.G. Basso, J. Hebling, C.A. de Souza Costa, Biological analysis of simvastatin-releasing chitosan scaffold as a cell-free system for pulp–dentin regeneration, J Endod 44 (2018) 971–976.e1.
[37] D.G. Soares, E.A.F. Bordini, F.B. Cassiano, E.S. Bronze-Uhle, L.E. Pacheco, G. Zabeo, J. Hebling, P.N. Lisboa-Filho, M.C. Bottino, C.A. de Souza Costa, Characterization of novel calcium hydroxide-mediated highly porous chitosan–calcium scaffolds for potential application in dentin tissue engineering, J. Biomed. Mater. Res. Part B 108 (2020) 2546–2559.
[38] D.G. Soares, E.A.F. Bordini, E.S. Bronze-Uhle, F.B. Cassiano, I.S.P. Silva, M. O. Gallinari, H.R. Matheus, J.M. Almeida, L.T.A. Cintra, J. Hebling, C.A. de Souza Costa, Chitosan-calcium-simvastatin scaffold as an inductive cell-free platform, J. Dent. Res. 100 (2021) 1118–1126.
[39] E.A.F. Bordini, F.B. Cassiano, E.S. Bronze-Uhle, L. Alamo, J. Hebling, C.A. de Souza Costa, D.G. Soares, Chitosan in association with osteogenic factors as a cell-homing platform for dentin regeneration: analysis in a pulp-in-a-chip model, Dent. Mater. 38 (2022) 655–669.
[40] K. El Kholy, M. Freire, T. Chen, T.E. Van Dyke, Resolvin E1 promotes bone preservation under inflammatory conditions, Front. Immunol. 9 (2018) 1300.
[41] D.J.R. Gusman, E. Ervolino, L.H. Theodoro, V.G. Garcia, M.J.H. Nagata, B.E. S. Alves, N.J. de Araujo, H.R. Matheus, J.M. de Almeida, Antineoplastic agents exacerbate periodontal inflammation and aggravate experimental periodontitis, J. Clin. Periodontol. 46 (2019) 457–469.
[42] P.C. Chang, W.C. Tai, H.T. Luo, C.H. Lai, H.H. Lin, Z.J. Lin, Y.C. Chang, B.S. Lee, Core–shell poly(D,L-lactide-co-glycolide)–chitosan nanospheres with simvastatin–doxycycline for periodontal and osseous repair, Int. J. Biol. Macromol. 158 (2020) 627–635.
[43] H. Qi, K. Wang, M. Li, Y. Zhang, K. Dong, S. Heise, A.R. Boccaccini, T. Lu, Co-culture of BMSCs and HUVECs with simvastatin-loaded gelatin nanosphere/chitosan coating on Mg alloy for osteogenic differentiation and vasculogenesis, Int. J. Biol. Macromol. 193 (2021) 2021–2028.
[44] W.K. Delan, I.H. Ali, M. Zakaria, B. Elsaadany, A.R. Fares, A.N. ElMeshad, W. Mamdouh, Investigating the bone regeneration activity of PVA nanofibers scaffolds loaded with simvastatin/chitosan nanoparticles in an induced bone defect rabbit model, Int. J. Biol. Macromol. 222 (2022) 2399–2413.
[45] M. Tavakoli, H. Salehi, R. Emadi, J. Varshosaz, S. Labbaf, A.M. Seifalian, F. Sharifianjazi, M. Mirhaj, 3D printed polylactic acid-based nanocomposite

scaffold stuffed with microporous simvastatin-loaded polyelectrolyte for craniofacial reconstruction, Int. J. Biol. Macromol. 258 (2024) 128917.
[46] A.G. Kurian, N. Mandakhbayar, R.K. Singh, J.H. Lee, G. Jin, H.-W. Kim, Multifunctional dendrimer@nanoceria engineered GelMA hydrogel accelerates bone regeneration through orchestrated cellular responses, Mater. Today Bio 20 (2023) 100664.
[47] D.M. Dos Santos, J.I. Moon, D.S. Kim, N.J. Bassous, C.A. Marangon, S.P. Campana-Filho, D.S. Correa, M.H. Kang, W.J. Kim, S.R. Shin, Hierarchical chitin nanocrystal-based 3D printed dual-layer membranes hydrogels: a dual drug delivery nano-platform for periodontal tissue regeneration, ACS Nano 18 (2024) 24182–24203.
[48] A. Gupta, S.K. Mehta, I. Qayoom, H.B. Jeon, A. Kumar, H.-W. Kim, Phyto-nanoengineered bone therapy with trans-resveratrol-gold nanoparticle cryogel scaffolds through modulating inflammatory reactions while stimulating bone regeneration, Chem. Eng. J. 525 (2025) 170314.
[49] S. Du, Y. Zheng, Y. Chen, Y. Guo, X. Kang, L. Wang, Fighting periodontitis with a pH-triggered nanocoating: A sustained-release strategy for simvastatin delivery, Colloids Surf. B Biointerfaces 260 (2026) 115375.
[50] F.B. Cassiano, D.G. Soares, E.A.F. Bordini, G. Anovazzi, J. Hebling, C.A.S. Costa, Simvastatin-enriched macro-porous chitosan–calcium–aluminate scaffold for mineralized tissue regeneration, Braz. Dent. J. 31 (2020) 385–391.
[51] M. Rafiq, J. Ahmed, H.A. Alturaifi, N.S. Awwad, H.A. Ibrahium, S. Mir, A. Maalik, S. Sabahat, S. Hassan, Z.U.H. Khan, Recent developments in the biomedical and anticancer applications of chitosan derivatives, Int. J. Biol. Macromol. 283 (2024) 137601.
[52] O. Fromigué, E. Hay, D. Modrowski, S. Bouvet, A. Jacquel, P. Auberger, P.J. Marie, RhoA GTPase inactivation by statins induces osteosarcoma cell apoptosis by inhibiting p42/p44-MAPKs–Bcl-2 signaling independently of BMP-2 and cell differentiation, Cell Death Differ. 13 (2006) 1845–1856.
[53] M. Yamashita, F. Otsuka, T. Mukai, H. Otani, K. Inagaki, T. Miyoshi, J. Goto, M. Yamamura, H. Makino, Simvastatin antagonizes tumor necrosis factor-alpha inhibition of bone morphogenetic proteins-2-induced osteoblast differentiation by regulating Smad signaling and Ras/rho-mitogen-activated protein kinase pathway, J. Endocrinol. 196 (2008) 601–613.
[54] N. Ghosh-Choudhury, C.C. Mandal, G.G. Choudhury, Statin-induced Ras activation integrates the phosphatidylinositol 3-kinase signal to Akt and MAPK for bone morphogenetic protein-2 expression in osteoblast differentiation, J. Biol. Chem. 282 (2007) 4983–4993.
[55] P.Y. Chen, J.S. Sun, Y.H. Tsuang, M.H. Chen, P.W. Weng, F.H. Lin, Simvastatin promotes osteoblast viability and differentiation via Ras/Smad/Erk/BMP-2 signaling pathway, Nutr. Res. 30 (2010) 191–199.
[56] I.S. Kim, B.C. Jeong, O.S. Kim, Y.J. Kim, S.E. Lee, K.N. Lee, J.T. Koh, H.J. Chung, Lactone form 3-hydroxy-3-methylglutaryl-coenzyme A reductase inhibitors (statins) stimulate the osteoblastic differentiation of mouse periodontal ligament cells via the ERK pathway, J. Periodontal Res. 46 (2011) 204–213.
[57] I. Fasolino, M.G. Raucci, A. Soriente, C. Demitri, M. Madaghiele, A. Sannino, L. Ambrosio, Osteoinductive and anti-inflammatory properties of chitosan-based scaffolds for bone regeneration, Mater. Sci. Eng. C 105 (2019) 110046.
[58] K. Sakoda, M. Yamamoto, Y. Negishi, J.K. Liao, K. Node, Y. Izumi, Simvastatin decreases IL-6 and IL-8 production in epithelial cells, J. Dent. Res. 85 (2006) 520–523.
[59] S. Emani, G.V. Gunjiganur, D.S. Mehta, Determination of the antibacterial activity of simvastatin against periodontal pathogens *Porphyromonas gingivalis* and *Aggregatibacter actinomycetemcomitans*: an in vitro study, Contemp. Clin. Dent. 5 (2014) 377–382.
[60] R. Kumar, S.N. Atluri, A. Achanta, C. Bogishetty, T.R. Chunduri, T. Pss, R. Ravi, Efficacy of simvastatin in inhibiting bone resorption and promoting healing in delayed tooth avulsion: a case series, Cureus 17 (2025) e79139.
[61] H. Betha, M. Rajmohan, R. Thakkar, B.R. Surya, M. Shetty, P. Sankla, R. Tiwari, Evaluation of crestal bone levels using simvastatin as an adjuvant around immediate implants: a clinico-radiographic study, J. Pharm. Bioallied Sci. 16 (2024) S279–S282.